Journal of
Applied Crystallography
ISSN 1600-5767

EXAFS investigation of the role of Cu on the chemical order and lattice distortion in $L1_0$ Fe–Pt–Cu thin films

S. Laureti, C. Brombacher, D. Makarov, M. Albrecht, D. Peddis, G. Varvaro and F. D'Acapito

J. Appl. Cryst. (2014). **47**, 1722–1728

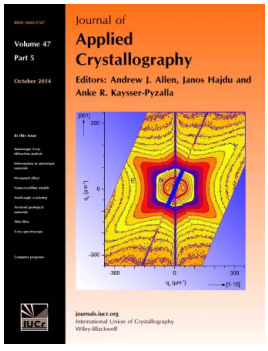

Many research topics in condensed matter research, materials science and the life sciences make use of crystallographic methods to study crystalline and non-crystalline matter with neutrons, X-rays and electrons. Articles published in the *Journal of Applied Crystallography* focus on these methods and their use in identifying structural and diffusion-controlled phase transformations, structure-property relationships, structural changes of defects, interfaces and surfaces, *etc.* Developments of instrumentation and crystallographic apparatus, theory and interpretation, numerical analysis and other related subjects are also covered. The journal is the primary place where crystallographic computer program information is published.

Journal of
Applied Crystallography
ISSN 1600-5767

Received 6 March 2014
Accepted 26 August 2014

EXAFS investigation of the role of Cu on the chemical order and lattice distortion in $L1_0$ Fe–Pt–Cu thin films

S. Laureti,[a]* C. Brombacher,[b] D. Makarov,[b]‡ M. Albrecht,[b]¶ D. Peddis,[a] G. Varvaro[a] and F. D'Acapito[c]

[a]Istituto di Struttura della Materia – CNR, 00016 Monterotondo Scalo, Rome, Italy, [b]Institute of Physics, Chemnitz University of Technology, D-09107 Chemnitz, Germany, and [c]CNR-IOM-OGG c/o ESRF, GILDA CRG, C/o ESRF BP220, F-38043 Grenoble, France. Correspondence e-mail: sara.laureti@ism.cnr.it

This work presents an extended X-ray absorption fine structure (EXAFS) characterization of ternary Fe–Pt–Cu alloys with different Cu content. The EXAFS measurements have been carried out at the Cu $K\alpha$ and Pt L_{III} edges in order to describe the local environment around these elements in the Fe–Pt–Cu samples and to compare the structural evolution as a function of the Cu content. The EXAFS study, based on a substitutional model where the Cu atoms occupy Fe or Pt sites in the tetragonal structure, has been performed by using linear dichroism to enhance the sensitivity to differently oriented bonds and to gain a detailed description of the atomic environment. The study allowed the effects on the chemical order and lattice distortion induced by the Cu atoms to be distinguished experimentally. The determined positions of the Cu atoms in the chemically $L1_0$-ordered face-centred tetragonal lattice were correlated with the magnetic properties of Fe–Pt–Cu ternary alloys. In particular, the main effect of Cu atoms in the alloy is a linear reduction of the c/a ratio, while the nonmonotonic behaviour of the chemical order is consistent with the variation of the magnetocrystalline anisotropy.

1. Introduction

Magneto-recording using hard disk drives is the dominant technology for storing information. To further improve its performance, new materials and technologies (Weller *et al.*, 2013; Shiroishi *et al.*, 2009; Piramanayagam & Chong, 2012) are needed to meet the critical requirements of the so-called 'magneto-recording trilemma', which consists in the trade-off between thermal stability, writability and high signal-to-noise ratio (Richter & Harkness, 2006). For this purpose, the development and optimization of new materials as recording media is the key task in the community to assure future success of magnetic data storage.

The equiatomic chemically ordered $L1_0$ alloys remain the most promising materials for future ultra-high-density perpendicular magnetic recording media beyond 1 Tbits per square inch (1 inch = 25.4 mm) owing to their high uniaxial magnetocrystalline anisotropy (K_u = 6.6–10 × 10^7 erg cm^{-3}, 1 erg = 10^{-7} J) (Weller *et al.*, 2000), which enables them to be thermally stable even at grain sizes down to 3 nm. Indeed, the peculiar structure of the $L1_0$ phase, as in the case of Fe–Pt alloys, where planes of pure Fe or Pt alternate along the [001] direction (c axis), is responsible of the strong anisotropy along the stacking direction that is generally interpreted as being due to the large spin-orbit coupling and a strong hybridization of the Pt 5d bands with highly polarized 3d bands of the transition metal (Cebollada *et al.*, 2002; Grange *et al.*, 2000).

Recently, advanced computational facilities have made it possible to analyse the dependence of the magnetocrystalline anisotropy energy as a function of the $L1_0$ structure. In particular, first principles electronic structure calculations, presented by Brown *et al.* (2003), revealed the existence of a competition between ferromagnetic (FM) and antiferromagnetic (AFM) spin structures in the Fe–Pt alloy. In their study, the FM state is energetically favoured by a decrease in the lattice distortion and/or in the degree of chemical order, *i.e.* as the system becomes more cubic. The chemical disorder with Pt atoms on Fe sites stabilizes the FM state, while perfectly chemically ordered Fe–Pt with the lowest c/a ratio (0.965) prefers an AFM state, where the Fe atoms have their spins on alternating planes with antiparallel spin configuration. Actually, at a given temperature and pressure, the equilibrium magnetic configuration is dependent on the interatomic distance between adjacent 3d transition elements as theoretically calculated by Lu *et al.* (2010). By varying the c/a lattice ratio, the distance between atomic planes along the c

‡ Present address: Institute for Integrative Nanosciences, Leibniz Institute for Solid State and Materials Research (IFW Dresden), Helmholtzstrasse 20, D-01069 Dresden, Germany.
¶ Present address: Institute of Physics, Augsburg University, Universitätstrasse 1, D-86135 Augsburg, Germany.

axis varies and, for large variations, results in a transition from the FM to the AFM state, due to the shortening of the Fe–Fe distance, and in a nonmonotonic behaviour of the magnetocrystalline anisotropy.

Many studies have been carried out to find the optimum conditions for the preparation of $L1_0$-ordered Fe–Pt alloys in the form of nanoparticles (Sun *et al.*, 2000; Sun, 2006; Capobianchi *et al.*, 2009; Liscio, Makarov *et al.*, 2010), nanorods (da Silva & Varanda, 2011; Poudyal *et al.*, 2009), thin films (Casoli *et al.*, 2005), patterned systems (Goll & Bublat, 2013; Kikitsu *et al.*, 2013) or capped magnetic structures (Makarov *et al.*, 2008; Albrecht & Makarov, 2012). The systems are commonly obtained by post-deposition high-temperature treatments for a few hours in order to favour the conversion from the chemically disordered and magnetically soft face-centred cubic (A1) phase into the chemically ordered and hard face-centred tetragonal (f.c.t., $L1_0$) phase.

It is well established, from an experimental point of view, that the chemical ordering, the lattice distortion (in particular the c/a ratio) and the magnetic anisotropy are strictly correlated, and they can be controlled by post-deposition thermal treatments and/or by the addition of a third element that reduces the temperature needed for the A1 to $L1_0$ transformation (Hsu *et al.*, 2001; Maeda *et al.*, 2002). As an example, it has been recently shown that the addition of Cu at different concentrations allows one to tailor the magnetocrystalline anisotropy (Brombacher *et al.*, 2012; Gilbert *et al.*, 2013) and decrease the Curie temperature (Berry & Barmak, 2007), which are the most important parameters for the technological application of these materials. For these systems, a careful determination of the structural and atomic arrangement becomes essential in order to understand the influence of the additional elements on the magnetic properties.

Among the characterization techniques applied to investigate the structural properties at the local scale, X-ray absorption spectroscopy (XAS) is an effective tool to probe the chemical environment around an absorber element and to get information on the average structural features of materials. XAS is thus complementary to conventional X-ray diffraction (XRD) techniques (Srajer *et al.*, 2006). Owing to its peculiar characteristics, *i.e.* selectivity and high sensitivity, extended X-ray absorption fine structure (EXAFS) analysis is the main technique used to investigate the local properties in many systems whose behaviour is strongly affected by the atomic arrangement. This is the case for the $L1_0$ or $L1_2$ chemically ordered alloys, where the degree of chemical order influences significantly the magnetocrystalline anisotropy (Meneghini *et al.*, 1999; Krupinski *et al.*, 2011; Blanc *et al.*, 2013; Liscio, Maret *et al.*, 2010).

A previous characterization of the long-range chemical order on Fe–Pt–Cu film samples has been carried out using anomalous X-ray diffraction (AXD) measurements in order to highlight the influence of the addition of Cu on the structural and magnetic properties (Maret *et al.*, 2012). In that study, two series of samples with different Cu content were prepared by a post-deposition rapid thermal annealing treatment at 873 and 1273 K for 30 s (Brombacher *et al.*, 2012). The samples were analysed by a tuneable synchrotron radiation source at the Fe K and Pt $L_{\rm III}$ edges in order to assess the long-range order parameter, which strongly affects the magnetocrystalline anisotropy. The results gave evidence of a tetragonal distortion of the lattice, more pronounced in the 873 K-annealed samples, due to the addition of Cu atoms, preferentially placed on the Fe lattice sites.

In this work, a careful EXAFS analysis on Fe–Pt–Cu samples with different Cu content has been carried out at the Cu $K\alpha$ and Pt $L_{\rm III}$ edges by using linear dichroism to enhance the sensitivity to differently oriented bonds and to obtain a detailed picture of the atomic environment around the two absorber atoms. Here, we take advantage of a local-scale characterization technique (complementary to AXD), whose sensitivity allows the study at the K edge of the diluted element, to characterize the Cu atomic arrangement in the samples annealed at 873 K and to confirm the structural variations observed as a function of the alloy composition. Moreover, the correlation of the EXAFS results with the magnetic behaviour of this system made it possible to experimentally distinguish the effect of the chemical order and structural distortions on the magnetocrystalline anisotropy, which is the key parameter for the technological application of these systems.

2. Experimental

Bilayers of $Fe_{52}Pt_{48}$[(50 − d) Å]/Cu[d Å], 50 Å thick, were sputter deposited at room temperature on thermally oxidized Si(100) substrates with a 1000 Å-thick amorphous SiO_2 layer. The Cu layer thickness d was varied from 0 to 12 Å, obtaining samples of different atomic composition as subsequently determined by Rutherford backscattering (in the following, we refer to samples Cu00, Cu04, Cu09, Cu15 and Cu21, indicating the amount of Cu in at.%). The as-grown samples were treated by rapid thermal annealing (RTA) at 873 K for 30 s in order to transform the Fe–Pt/Cu bilayer into a ternary Fe–Pt–Cu alloy, exhibiting a chemically ordered f.c.t. phase ($L1_0$) with (001) texture and strong perpendicular magnetic anisotropy (Brombacher *et al.*, 2012).

XAS data were collected at the GILDA-CRG beamline at the ESRF (Grenoble, France) (D'Acapito *et al.*, 1998). The monochromator was equipped with a pair of Si(111) crystals used in dynamical focusing mode. A pair of Pd-coated mirrors was used for harmonic rejection and vertical beam focusing. Data collection was carried out at the Cu $K\alpha$ (8980 eV) and Pt $L_{\rm III}$ (11 564 eV) edges with the polarization vector of the X-ray beam either parallel or perpendicular to the sample surface. The angle between the X-ray polarization vector and the normal to the surface was 90° in the 'parallel' and 15° in the 'perpendicular' configuration, and this permitted also the minimization of the coherent scattering signal from the Si substrate and the enhancement of the fluorescence from the atoms under study. During data collection, the samples were kept at a temperature of 100 K to reduce the thermal atomic vibrations, thus enhancing the EXAFS signal. The absorption coefficient was measured *via* the fluorescence yield from

Cu $K\alpha$ or Pt L_{III} lines using an energy-resolving 13-element high-purity germanium detector (energy resolution of about 250 eV).

All samples were measured by collecting data sets in the parallel and perpendicular configurations to enhance the sensitivity to differently oriented bonds for the two cases, which provides a more detailed description of the atomic environment within the alloy. Despite the lower polarization sensitivity of the EXAFS signal at the Pt L_{III} edge with respect to the K edges (see details later), the high degree of chemical ordering along the (001) direction, as shown by the XRD analysis (Brombacher *et al.*, 2012), allowed the detection of orientational dicroism at the absorption edges (Meneghini *et al.*, 1999). Data were also collected at the Fe K edge, but a considerable signal from an oxide phase (not present on the other edges) on the film surface prevented a careful structural analysis and thus it was not considered in the subsequent study. All the analyses have been carried out by assuming a substitutional model (ruling out the possibility to have interstitial Cu), as suggested by previous theoretical calculations and experimental studies (Kai *et al.*, 2004; Maret *et al.*, 2012) where a preferential Cu on Fe (Cu_{Fe}) site was found. XAS data extraction and fitting were carried out with the *ATHENA* and *ARTEMIS* codes (Ravel & Newville, 2005), while quantitative modelling was based on simulated EXAFS signals using the *FEFF8.1* code (Ankudinov *et al.*, 1998).

3. Results and discussion

The analysis of the first coordination shell around the absorber Pt atom was carried out at the Pt L_{III} edge with the aim of studying the effect of the Cu concentration on the ordering degree of the $L1_0$ alloy.

For this purpose, data acquired in both parallel and perpendicular configurations were simultaneously fitted with a model based on a linear combination of single scattering paths for the direct structure (Pt as central atom in a ideal chemically $L1_0$-ordered Fe–Pt tetragonal cell: 8Pt–Fe paths and 4Pt–Pt paths) and single scattering paths for the reverse structure, where the Pt absorber atom occupies an Fe site (8Pt–Pt paths and 4 Pt–Fe paths, simulating the effect of chemical disorder). In Fig. 1, a sketch of the first neighbours in the two configurations is presented. Depending on the angle Θ between the beam polarization and the bond direction, atoms contribute differently to the amplitude of the associated XAS signal. For the K edge the dependence is $3\cos^2\Theta$, whereas for the $L_{II,III}$ edges it is of the type $A + B\cos^2\Theta$ (Heald & Stern, 1977). As an example, the atoms (white circles) lying on a plane perpendicular to the beam direction in the parallel configuration (which correspond to the Fe atoms in the direct structure) do not give any contribution to the signal amplitude at the K edge, the angle between the bonds and the beam direction being 90°; on the other hand, each atom contributes to the absorption signal in the perpendicular configuration, with an amplitude proportional to $\cos^2\beta$. In any case, the calculations of the theoretical XAS signals were carried out including the polarization effects depending on the specific absorption edge, as implemented in the *FEFF* code. It has to be noted that the Pt–Cu paths were not considered in the model since the detectable signal would have been less than one atom even in the most concentrated sample. The quantitative analysis was performed in the Fourier-transformed space (R space) in the range R = [1.7–3.4] Å, for the k^2-weighted EXAFS data using Hanning windows with a slope parameter dk = 1. The free fitting parameters used in the analysis are the Pt—Pt and Pt—Fe distances, the shift of the energy origin ΔE_0, the Debye–Waller factors (DWFs), and a chemical order parameter X, which represents the degree of chemical order, being equal to zero for a chemically disordered configuration (50% of direct structure and 50% of reverse structure) and equal to 1 for a chemically ordered configuration (100% of direct structure). In order to minimize the number of free parameters, the DWFs were calculated with a correlated Debye model (Zabinsky *et al.*, 1995) with a single temperature value (denoted as CDMT parameter), accounting for the DWFs of the Pt—Pt and Pt—Fe bonds; moreover, the Pt—Pt distance for the direct structure (r_1) was set equal to the Pt—Fe distance for the reverse structure, while r_2 represents the Pt—Fe distance in the direct structure and the Pt—Pt distance in the reverse structure.

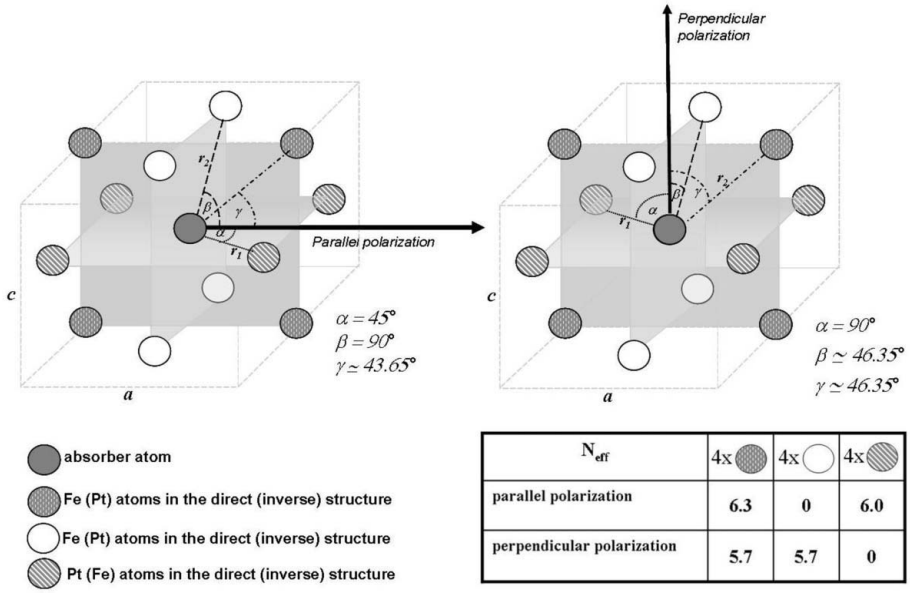

N_{eff}	4x	4x	4x
parallel polarization	6.3	0	6.0
perpendicular polarization	5.7	5.7	0

Figure 1
Crystallographic structure of the first coordination shell around the Pt absorber atom in the $L1_0$ structure in the parallel and perpendicular configurations. For the sake of simplicity, the values of the effective coordination number are calculated only for a generic K absorption edge.

In Fig. 2 the EXAFS signals at the Pt L_{III} edge and the relative Fourier transform (FT) are reported for both the parallel (*a*), (*b*) and the perpendicular (*c*), (*d*) configurations for all samples. It is worth noting that the good EXAFS data in a wide k range up to 16 Å^{-1} allowed the high-quality fitting of the main FT peak, which represents the first coordination shell around the absorber atom.

The results summarized in Table 1 show that the presence of Cu in the alloy affects the chemical ordering, favouring the A1 to $L1_0$ phase transition, as previously demonstrated by electron diffraction measurements performed on the same set of samples (Brombacher *et al.*, 2012); in particular, the EXAFS analysis indicates a nonmonotonic behaviour, as demonstrated by the chemical order parameter X, which increases up to a value of 0.9 for Cu09 and then decreases for higher Cu concentrations. The results are in good agreement with the corresponding magnetic properties (Brombacher *et al.*, 2012), showing a similar behaviour of the magnetocrystalline anisotropy as a function of Cu content (Fig. 3). This demonstrates that it is possible to tune the chemical order and thus the magnetic anisotropy by varying the Cu content, and that the best conditions are found for a Cu content of about 10 at.%.

Table 1
Structural parameters for the first coordination shell obtained from the simultaneous fit of the EXAFS Pt L_{III} signals in parallel and perpendicular configurations.

r_1 represents the Pt—Pt distance for the direct structure and the Pt—Fe distance for the reverse structure. r_2 represents the Pt—Fe distance in the direct structure and the Pt—Pt distance in the reverse structure. The temperature from the correlated Debye model (CDMT) accounts for the disorder of the bond lengths, while the X parameter represents the degree of chemical order (equal to zero for 50% of direct structure and 50% of reverse structure and equal to 1 for 100% of direct structure).

Sample	r_1 (Å) (theory 2.758 Å)	r_2 (Å) (theory 2.695 Å)	CDMT (K)	X
Cu00 (no Cu)	2.756 (9)	2.693 (7)	230 (30)	0.5 (2)
Cu04	2.759 (5)	2.676 (5)	290 (30)	0.7 (1)
Cu09	2.770 (6)	2.660 (5)	300 (30)	0.9 (1)
Cu15	2.773 (6)	2.662 (4)	320 (40)	0.7 (1)
Cu21	2.768 (5)	2.646 (4)	350 (50)	0.6 (1)

In addition to the chemical ordering, the EXAFS analysis revealed the structural evolution concerning the tetragonality of the formed alloy: by increasing the Cu content, the first peak of the FT in the perpendicular configuration, which corresponds to the Pt—Pt distance in the first nearest-neigh-

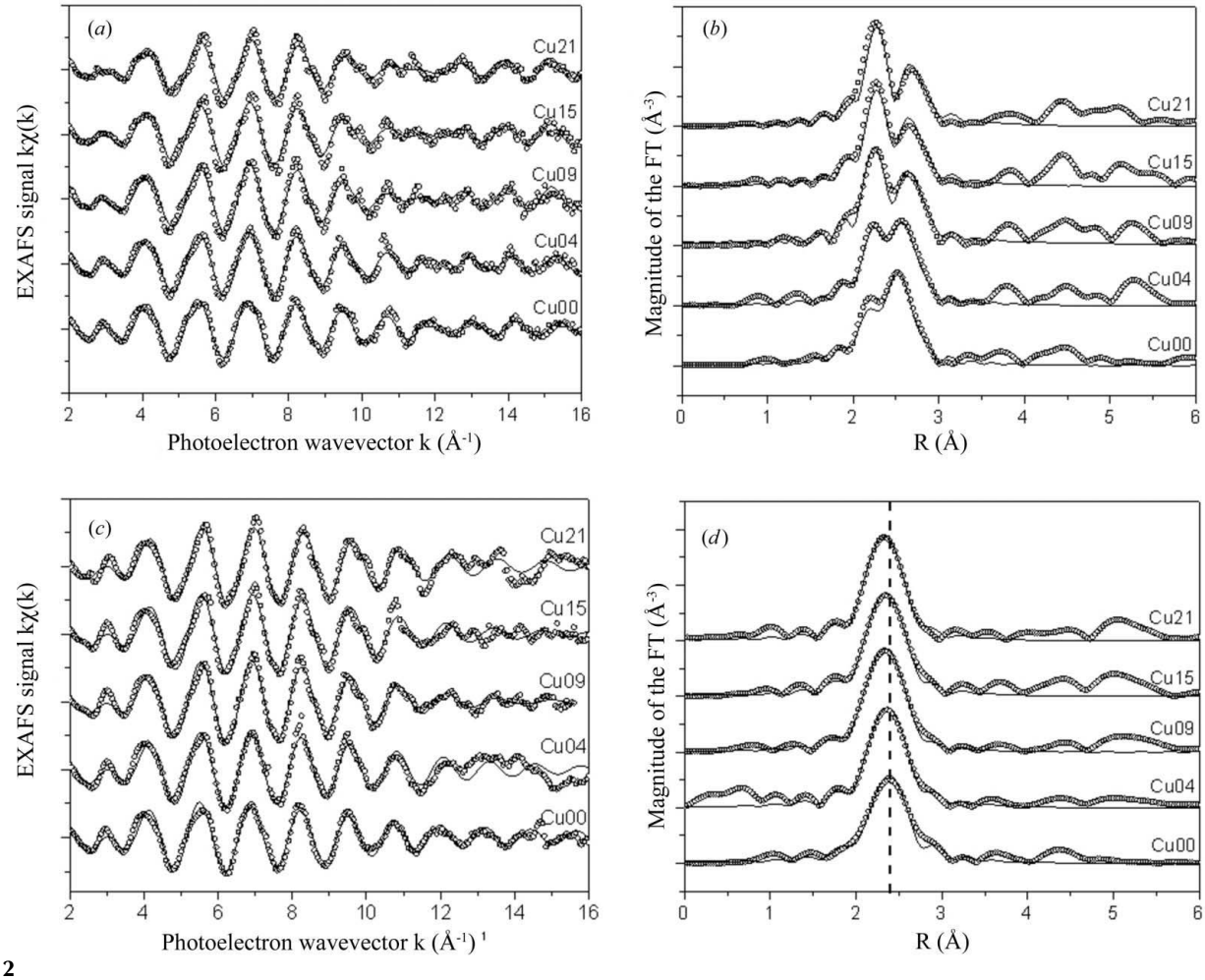

Figure 2
EXAFS signals (left) at the Pt L_{III} edge and the relative Fourier transform (right) obtained in the parallel (*a*), (*b*) and perpendicular (*c*), (*d*) configurations. Experimental data (open circles) and fit (solid lines).

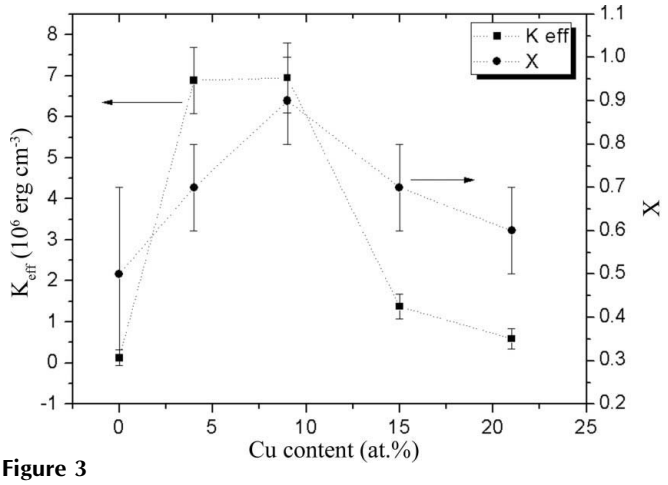

Figure 3
Comparison between the magnetocrystalline effective magnetic anisotropy constant K_{eff} (left) and the chemical order parameter X (right) as a function of the Cu content.

bour shell (*i.e.* the *c* lattice parameter), moves towards lower values (Fig. 2*d*). Contrary to what has been observed for the chemical order, the contraction of the tetragonal axis increases linearly with Cu content. The *a* and *c* lattice parameters were quantitatively evaluated from the r_1 and r_2 distances, by considering that $a = 2r_1\cos\alpha$ and $c = 2(r_2^2 - r_1^2\cos^2\alpha)^{1/2}$. The obtained values of the tetragonality ratio *c*/*a* are in good agreement with the XRD data (Table 2).

Table 2
Comparison between lattice parameters and the *c*/*a* ratio obtained by XRD (Brombacher *et al.*, 2012) analysis and EXAFS fit at the Pt L_{III} edge.

	a		*c*		*c*/*a*	
Sample	XRD	EXAFS	XRD	EXAFS	XRD	EXAFS
Cu04	3.92 (2)	3.90 (2)	3.67 (1)	3.66 (1)	0.94 (1)	0.94 (1)
Cu09	3.94 (2)	3.92 (2)	3.62 (1)	3.60 (1)	0.92 (1)	0.92 (1)
Cu15	3.94 (2)	3.92 (2)	3.58 (1)	3.60 (1)	0.91 (1)	0.92 (1)
Cu21	3.95 (2)	3.94 (2)	3.54 (1)	3.56 (1)	0.90 (1)	0.91 (1)

In order to study the first-shell atomic arrangement around the Cu atoms in the alloy, EXAFS data obtained at the Cu *Kα* edge (Fig. 4) were fitted in the Fourier-transformed space in the range [1.4–3.4] Å, where only the nearest-neighbour contributions are included for the k^2-weighted EXAFS data in the range [3.0–14.0] Å using Hanning windows with a slope parameter d*k* = 1. The comparison of these spectra with

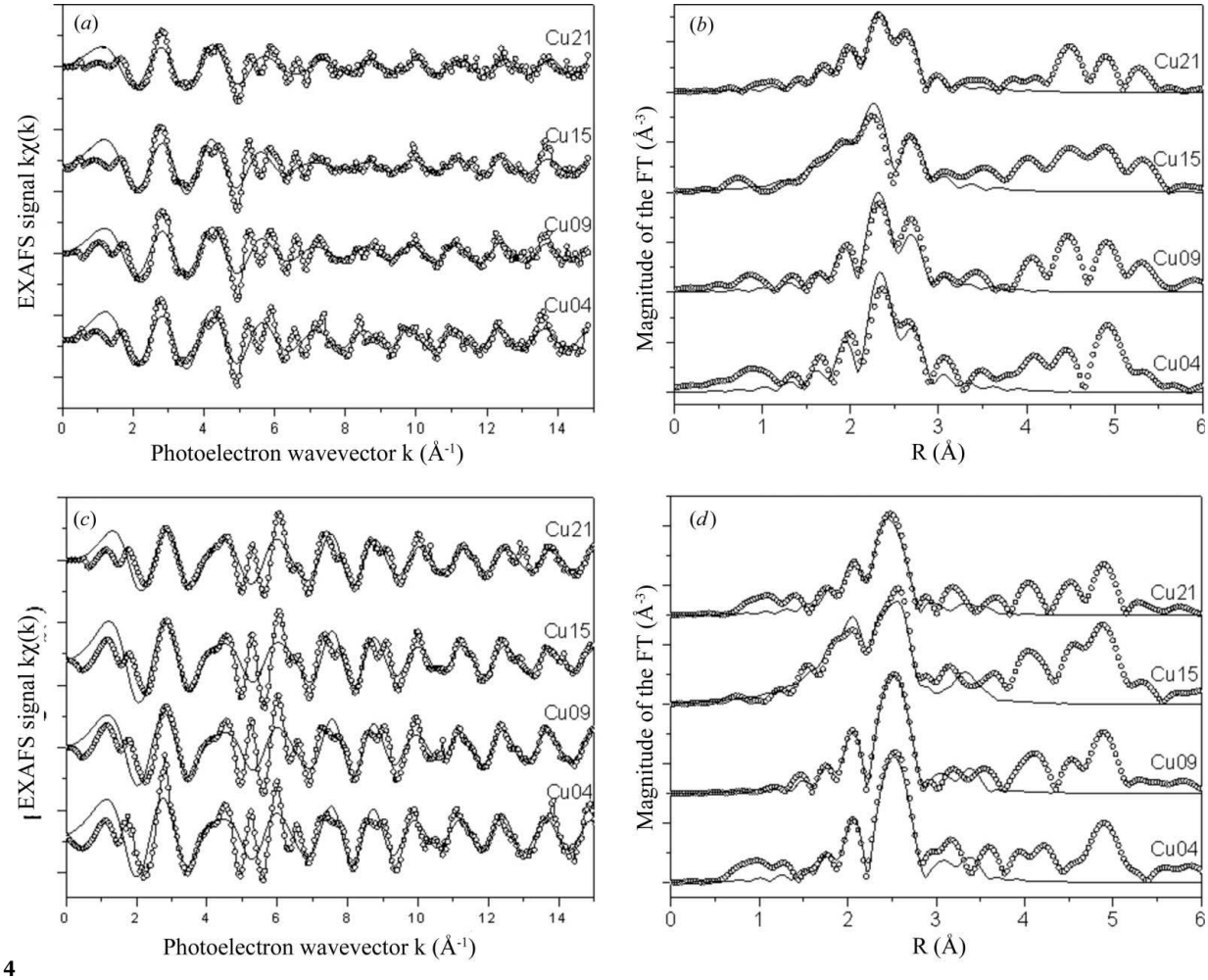

Figure 4
EXAFS signals (left) at the Cu *Kα* edge and the relative Fourier transform (right) obtained in the parallel (*a*), (*b*) and perpendicular (*c*), (*d*) configurations. Experimental data (open circles) and fit (solid lines).

Table 3
Structural parameters for the Cu first coordination shell obtained from the simultaneous fit of the EXAFS Cu *K* signals in parallel and perpendicular configurations (Fig. 4).

The r_{Cu-Fe} and r_{Cu-Pt} distances correspond to the Pt—Pt and Pt—Fe distances of the $L1_0$ direct structure; the temperature from the correlated Debye model (CDMT) accounts for the disorder of the bond lengths.

Sample	$\%Cu_{Fe}$	r_{Cu-Fe} (Å) (theory 2.758 Å)	r_{Cu-Pt} (Å) (theory 2.695 Å)	CDMT (K)
Cu04	0.91 (6)	2.72 (1)	2.651 (5)	310 (30)
Cu09	0.91 (3)	2.758 (9)	2.646 (3)	325 (20)
Cu15	0.93 (8)	2.73 (2)	2.639 (5)	265 (45)
Cu21	0.70 (6)	2.73 (2)	2.635 (6)	315 (35)

EXAFS data obtained for a pure metallic Cu bulk sample (see Eisenberger & Lengeler, 1980) indicates the absence of Cu segregation or agglomeration even in the more concentrated sample. Thus, considering a substitutional model, scattering paths were calculated after creating substitutional defects Cu_{Fe} and Cu_{Pt} in the Fe–Pt $L1_0$ structure. The paths were generated for both parallel and perpendicular configurations and, for each sample, the two data sets were simultaneously fitted by a model based on a linear combination of the two structures. The overall amplitudes for these two cases are a measure of the percentage of Cu on Fe or Pt sites. The free fitting parameters used in the analysis are the Cu—Pt and Cu—Fe distances, the amplitudes (*i.e.* the percentage of Cu_{Fe} and Cu_{Pt}), and the DWFs.

The first-shell analysis revealed that, for a Cu concentration up to 15 at.%, the Cu atoms are predominantly located at the Fe sites, while for higher concentrations they start to occupy also the Pt sites (Table 3). The present study did not allow elucidation of the specific role of the Fe atoms; however, the tendency toward a random atomic distribution at higher concentration is consistent with previous structural investigations by anomalous X-ray scattering (Maret *et al.*, 2012) carried out close to the Fe *K* and Pt L_{III} edges on a series of samples with the same compositions (but annealed at 1273 K). In that case, the effect of addition of Cu beyond 9 at.% was an atomic redistribution between the alternating Fe and Pt planes with a decrease of the order parameter.

By combining the analyses at the Cu $K\alpha$ and Pt L_{III} edges we are able to clearly elucidate the effect of Cu atoms on the structural properties of an alloy whose magnetic properties strongly depend on the Cu content, as previously shown (Brombacher *et al.*, 2012). In this study, we observed a linear reduction in the tetragonality ratio, *c*/*a*, from 0.92 (Cu04) to 0.89 (Cu21) and, at the same time, a nonmonotonic effect of the Cu amount on the chemical ordering, which correlates well with the trend of the effective anisotropy estimated from hysteresis loops (Fig. 3). This finding indicates that the magnetic response is mainly governed by the chemical ordering. Our results are in agreement with previous theoretical calculations and experiments (Lu *et al.*, 2010; Lyubina *et al.*, 2005), which indicate that the lattice distortion is expected to have a smaller influence on magnetic properties compared to the chemical ordering.

4. Conclusions

An EXAFS analysis performed on Fe–Pt–Cu film samples with different Cu content allowed the determination of the local order effect induced on the $L1_0$ structure. The significant polarization dependence of the absorption spectra confirmed the high degree of crystallographic order, as previously shown from both the magnetic characterization and XRD measurements. In particular, the analysis carried out at the Pt edge revealed that the chemical order around the Pt atoms is strongly influenced by the addition of Cu atoms, consistent with the variation of the magnetocrystalline anisotropy. On the other hand, the effect of Cu atoms in the alloy is a lattice distortion with a linear reduction of the *c*/*a* ratio, although this effect has a minor influence on the magnetocrystalline anisotropy when compared to the effect of the chemical ordering. The good quality of the absorption spectra and the quite simple substitutional model used to fit the EXAFS signals made this study complementary to the approaches usually applied to determine the long-range order and the structural parameters in $L1_0$ alloys. Moreover, this method represents a useful tool that is able to experimentally distinguish the effects of chemical ordering and lattice distortion through the study of a diluted third element in the $L1_0$ alloy, providing experimental support of theoretical predictions.

This work was supported by the European Commission FP7 project TERAMAGSTOR (contract No. FP7-ICT-2007-2-224001) and, in part, by MIUR under project FIRB2010 – NANOREST and the German Science Foundation (DFG) grant MA 5144/1-1. GILDA is a project jointly financed by CNR and INFN.

References

Albrecht, M. & Makarov, D. (2012). *Open Surface Sci. J.* **4**, 42–54.
Ankudinov, A. L., Ravel, B., Rehr, J. J. & Conradson, S. D. (1998). *Phys. Rev. B*, **58**, 7565–7576.
Berry, D. C. & Barmak, K. (2007). *J. Appl. Phys.* **102**, 024912.
Blanc, N., Díaz-Sánchez, L., Ramos, A., Tournus, F., Tolentino, H., De Santis, M., Proux, O., Tamion, A., Tuaillon-Combes, J., Bardotti, L., Boisron, O., Pastor, G. & Dupuis, V. (2013). *Phys. Rev. B*, **87**, 155412.
Brombacher, C., Schletter, H., Daniel, M., Matthes, P., Jöhrmann, N., Maret, M., Makarov, D., Hietschold, M. & Albrecht, M. (2012). *J. Appl. Phys.* **112**, 073912.
Brown, G., Kraczek, B., Janotti, A., Schulthess, T., Stocks, G. & Johnson, D. (2003). *Phys. Rev. B*, **68**, 052405.
Capobianchi, A., Colapietro, M., Fiorani, D., Foglia, S., Imperatori, P., Laureti, S. & Palange, E. (2009). *Chem. Mater.* **21**, 2007–2009.
Casoli, F., Albertini, F., Pareti, L., Fabbrici, S., Nasi, L., Bocchi, C. & Ciprian, R. (2005). *IEEE Trans. Magn.* **41**, 3223–3225.
Cebollada, A., Farrow, R. F. C. & Toney, M. F. (2002). *Magnetic Nanostructures*, ch. 3, p. 93. Stevenson Ranch: American Scientific Publishers.
D'Acapito, F. *et al.* (1998). *ESRF Newsl.* **30**, 42–44.
Eisenberger, P. & Lengeler, B. (1980). *Phys. Rev. B*, **22**, 3551–3562.
Gilbert, D. A., Wang, L., Klemmer, T. J., Thiele, J., Lai, C. & Liu, K. (2013). *Appl. Phys. Lett.* **102**, 132406.

Goll, D. & Bublat, T. (2013). *Phys. Status Solidi A*, **210**, 1261–1271.
Grange, W., Galanakis, I., Alouani, M. & Maret, M. (2000). *Phys. Rev. B*, **62**, 1157–1166.
Heald, S. & Stern, E. (1977). *Phys. Rev. B*, **16**, 5549–5559.
Hsu, Y.-N., Jeong, S., Laughlin, D. E. & Lambeth, D. N. (2001). *J. Appl. Phys.* **89**, 7068.
Kai, T., Maeda, T., Kikitsu, A., Akiyama, J., Nagase, T. & Kishi, T. (2004). *J. Appl. Phys.* **95**, 609–612.
Kikitsu, A., Maeda, T., Hieda, H., Yamamoto, R., Kihara, N. & Kamata, Y. (2013). *IEEE Trans. Magn.* **49**, 693–698.
Krupinski, M., Perzanowski, M., Polit, A., Zabila, Y., Zarzycki, A., Dobrowolska, A. & Marszalek, M. (2011). *J. Appl. Phys.* **109**, 064306.
Liscio, F., Makarov, D., Maret, M., Doisneau-Cottignies, B., Roussel, H. & Albrecht, M. (2010). *Nanotechnology*, **21**, 065602.
Liscio, F., Maret, M., Meneghini, C., Mobilio, S., Proux, O., Makarov, D. & Albrecht, M. (2010). *Phys. Rev. B*, **81**, 125417.
Lu, Z., Chepulskii, R. V. & Butler, W. H. (2010). *Phys. Rev. B*, **81**, 094437.
Lyubina, J., Opahle, I., Müller, K., Gutfleisch, O., Richter, M., Wolf, M. & Schultz, L. (2005). *J. Phys. Condens. Matter*, **17**, 4157–4170.
Maeda, T., Kai, T., Kikitsu, A., Nagase, T. & Akiyama, J. (2002). *Appl. Phys. Lett.* **80**, 2147.
Makarov, D., Brombacher, C., Liscio, F., Maret, M., Parlinska, M., Meier, S., Kappenberger, P. & Albrecht, M. (2008). *J. Appl. Phys.* **103**, 053903.
Maret, M., Brombacher, C., Matthes, P., Makarov, D., Boudet, N. & Albrecht, M. (2012). *Phys. Rev. B*, **86**, 024204.
Meneghini, C., Maret, M., Parasote, V., Cadeville, M. C., Hazemann, J. L., Cortes, R. & Colonna, S. (1999). *Eur. Phys. J. B*, **7**, 347–357.
Piramanayagam, S. N. & Chong, T. C. (2012). Editors. *Development in Data Storage, Materials Perspective.* New York: John Wiley and Sons.
Poudyal, N., Chaubey, G. S., Rong, C.-B. & Liu, J. P. (2009). *J. Appl. Phys.* **105**, 07A749.
Ravel, B. & Newville, M. (2005). *J. Synchrotron Rad.* **12**, 537–541.
Richter, H. & Harkness, S. (2006). *MRS Bull.* **31**, 384–388.
Shiroishi, Y., Fukuda, K., Tagawa, I., Iwasaki, H., Takenoiri, S., Tanaka, H., Mutoh, H. & Yoshikawa, N. (2009). *IEEE Trans. Magn.* **45**, 3816–3822.
Silva, T. L. da & Varanda, L. C. (2011). *Nano Res.* **4**, 666–674.
Srajer, G., Lewis, L., Bader, S., Epstein, A., Fadley, C., Fullerton, E., Hoffmann, A., Kortright, J., Krishnan, K. M., Majetich, S., Rahman, T., Ross, C., Salamon, M., Schuller, I., Schulthess, T. & Sun, J. (2006). *J. Magn. Magn. Mater.* **307**, 1–31.
Sun, S. (2006). *Adv. Mater.* **18**, 393–403.
Sun, S., Murray, C. B., Weller, D., Folks, L. & Moser, A. (2000). *Science*, **17**, 1989–1992.
Weller, D., Mosendz, O., Parker, G., Pisana, S. & Santos, T. S. (2013). *Phys. Status Solidi A*, **210**, 1245–1260.
Weller, D., Moser, A., Folks, L., Best, M., Lee, W., Toney, M., Schwickert, M., Thiele, J. & Doerner, M. (2000). *IEEE Trans. Magn.* **36**, 10–15.
Zabinsky, S., Rehr, J., Ankudinov, A., Albers, R. & Eller, M. (1995). *Phys. Rev. B*, **52**, 2995–3009.